ADVANCED FUNCTIONAL MATERIALS
www.afm-journal.de

Real-Time UVC Imaging and High Safety Communication Based on Dual-Detectable Lead-Free Perovskite Heterostructure

Fa Cao, Enliu Hong, Ziqing Li, Sancan Han, and Xiaosheng Fang**

Ultraviolet band C photodetectors (UVC PDs), which can convert the UVC light (200–280 nm) signals into detectable signals, have received tremendous attention due to their wide applications in bio-medicine, communications, and imaging fields. However, current research primarily focuses on either the conversion of UVC light into electrical signals or its conversion into visible light signals. Here, a flexible dual-detectable UVC PD based on $Ca_2Nb_3O_{10}$ nanosheets and $CsCu_2I_3$ film is reported, which can simultaneously convert UVC light into visible light and electrical signals, achieving the visual detection for invisible UVC light. The PD exhibits exceptional self-powered UVC light (270 nm; 1.87 mW cm^{-2}) detection abilities with a high responsivity (R) of 16.7 mA W^{-1}, an impressive detectivity of 6.1 × 10^{11} Jones, a high on/off ratio of 3789, and an ultra-high UVC/UVA (R_{270}/R_{360}) rejection ratio of 2.1 × 10^5. The dual-detectable PD shows great application potential for safety communication and real-time imaging. This work proposes a new type of flexible PD through material selection and structural design, thereby inspiring novel ideas to enhance the convenience and practicality of UVC photodetection.

1. Introduction

Ultraviolet (UV) light with a wavelength ranging from 10 to 400 nm is a double-edge sword to mankind,[1–3] and the UV radiation from the sun which can be further divided into three bands, named UVA (315–400 nm), UVB (280–315 nm), UVC (200–280 nm). On the one hand, excessive UV radiation can lead to skin aging and even cancer. On the other hand, UV radiation can be used for imaging, security communication, and medical cosmetology, etc.[4] Therefore, the detection of UV light has emerged as a prominent area of research to make better use of UV light for the benefit of human beings. When the UV light radiated by sunlight penetrates the atmosphere, the wavelength in the range of 200–280 nm will be absorbed by ozone in the atmosphere and rarely reach the earth's surface. There is no doubt that using UVC light for communication and imaging has higher security.[5]

Various UVC photodetector (PD) based on wide bandgap semiconductors (Sm_2O_3,[6] Diamond,[7] AlGaN,[8] and Ga_2O_3,[9] etc.) have been fabricated for the detection of UVC light and demonstrated preferable performance. For instance, solar-blind Sn-doped β-Ga_2O_3 microbelts show a responsivity of 300 A W^{-1} and a UVC/dark current ratio of 10^8 was reported by Shan's group.[9] Huang et al[6] demonstrate a p-Graphene/i-Sm_2O_3/n-SiC solar-blind UVC PD, exhibiting a self-powered responsivity of 19.8 mA W^{-1} and a detective as high as 1.2 × 10^{11} Jones. However, the above-mentioned PDs have poor flexibility and thus can not satisfy our daily demands for flexible devices.[10] Recent emerging 2D wide bandgap oxide perovskite nanosheets including $Ca_2Nb_3O_{10}$ (CNO) and $Sr_2Nb_3O_{10}$ (SNO), which show high flexible UVC light detection abilities have been reported by our group.[11,12] Nevertheless, previous reports mainly focus on the conversion of UVC light into electrical signals, which require corresponding electrical signal measuring equipment.[13,14] In some cases, we need to sense UVC light without the help of external devices.[15] Against this background, metal halide perovskites, especially non-toxic Cu-based perovskites ($CsCu_2I_3$ and $Cs_3Cu_2I_5$, named CCI123 and CCI325, respectively), have attracted much attention because of their defects or self-trapping exciton luminescence, enabling the conversion of UVC light into visible light.[16,17] For instance, Pan group[18] achieved the conversion of UVC light to yellow light through $CsCu_2I_3$ films. The ability to convert invisible UVC light to visible light could achieve visual detection of UVC light, simplifying our detection of UVC light

F. Cao
State Key Laboratory of Organic Electronics and Information Displays
Institute of Advanced Materials (IAM)
School of Materials Science and Engineering
Nanjing University of Posts and Telecommunication (NJUPT)
Nanjing 210023, P. R. China

F. Cao, E. Hong, Z. Li, X. Fang
Department of Materials Science
Institute of Optoelectronics, State Key Laboratory of Molecular Engineering of Polymers
Fudan University
Shanghai 200433, P. R. China
E-mail: xshfang@fudan.edu.cn

S. Han
School of Opto-electronic and Computer Engineering
University of Shanghai for Science and Technology
Shanghai 200093, P. R. China
E-mail: schan@usst.edu.cn

The ORCID identification number(s) for the author(s) of this article can be found under https://doi.org/10.1002/adfm.202422161

DOI: 10.1002/adfm.202422161

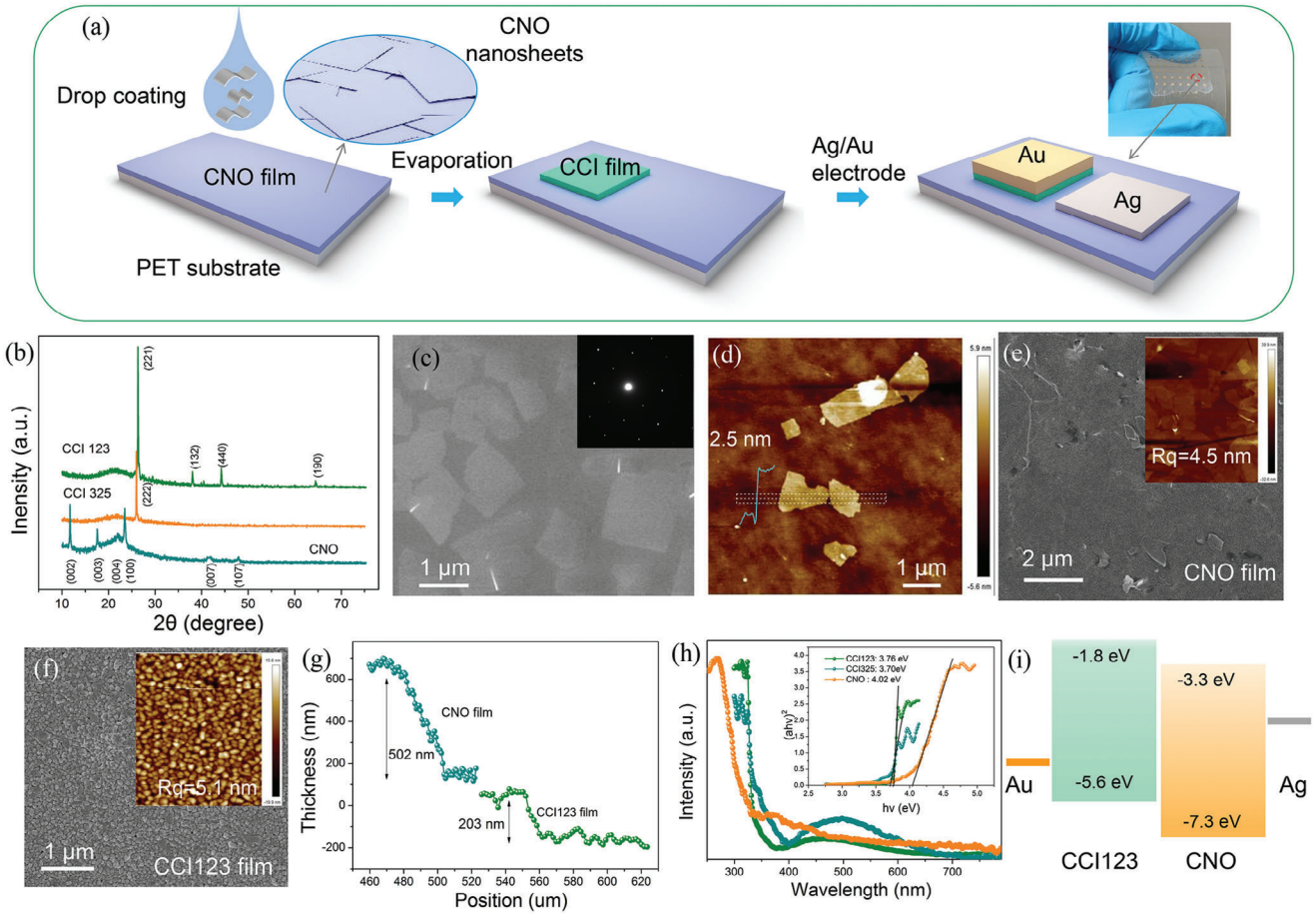

Figure 1. a) The fabrication steps of CNO/CCI123 UV PD on PET substrate. b) XRD spectra of CNO, CCI123, and CCI325 films. c,d) SEM and AFM images of CNO nanosheets and inset of c) is the corresponding SAED pattern. e,f) SEM images of CNO and CCI123 films, respectively and the inset is their corresponding AFM images. g) Height profiles of CNO and CCI123 films. h) Absorption spectra of CNO, CCI123, and CCI325 films and the inset is the energy bandgaps of CNO, CCI123, and CCI325 films. i) Energy band alignment of CNO and CCI123.

in some qualitative situations. However, to the best of our knowledge, there is a limited report available that specifically focuses on the dual detection (converting UVC light to electricity and visible light) of UVC light. With the rapid development of UVC photodetection technology, it's urgently needed to exploit novel devices with UVC dual detection ability to meet the demands for UVC light real-time imaging and quantitative test. The combination of 2D CNO nanosheets with Cu-based perovskites may realize the conversion of UVC light to electricity and visible light at the same time.

Inspired by current demands, a flexible UVC photodetector with dual-detectable capabilities was devised through the integration of 2D CNO nanosheets with $CsCu_2I_3$ films. The PD exhibits superior stability, self-powered characteristics, and excellent flexibility in detecting UVC light (270 nm; 1.87 mW cm^{-2}). Specifically, it demonstrates outstanding performance with a responsivity of 16.7 mA W^{-1}, detectivity of 6.1×10^{11} Jones, on/off ratio of 3789, and an ultra-high UVC/UVA (R_{270}/R_{360}) rejection ratio of 2.1×10^5, exhibiting great application potential for safety communication and real-time imaging. Our research and development of the UVC dual detection method can serve as a milestone in the field of UVC PDs.

2. Results and Discussion

The schematic of the fabrication procedures of the PD is shown in **Figure 1a**. The cleaned PET substrate is treated by air plasma for the following film deposition process. The CNO colloidal solution is dropped onto the PET substrate to ensure homogeneous diffusion of the solution, followed by drying at 60 °C to obtain a uniform CNO film composed of nanosheets. The CCI123 film was evaporated on the CNO film to form a heterojunction, then Au and Ag electrodes were deposited on CCI123 and CNO film, respectively. The flexible Au/CCI123/CNO/Ag UVC PD is shown in Figures 1a and S1 (Supporting Information). The X-ray diffractometer (XRD) spectra of CCI123, CCI325, and CNO films are shown in Figure 1b. The 2θ peaks located at 11.7°, 17.4°, 22.0°, 23.3°, 41.58°, and 47.96° can be attributable to the (002), (003), (004), (100), (007), and (107) crystal facets of tetragonal hydrogen calcium niobium oxide (PDF # 00-040-0884).[11,19] The obvious (00l) peaks demonstrated the layered structure of CNO nanosheets. For CCI325 films, the peaks located at 25.9° are assigned to (222) planes of $Cs_3Cu_2I_5$ (PDF # 79–0333).[20] While four peaks of CCI123 films with a 2θ values of 26.4°, 38.1°, 44.3°, and 64.6° can be attributable to the (221), (132),

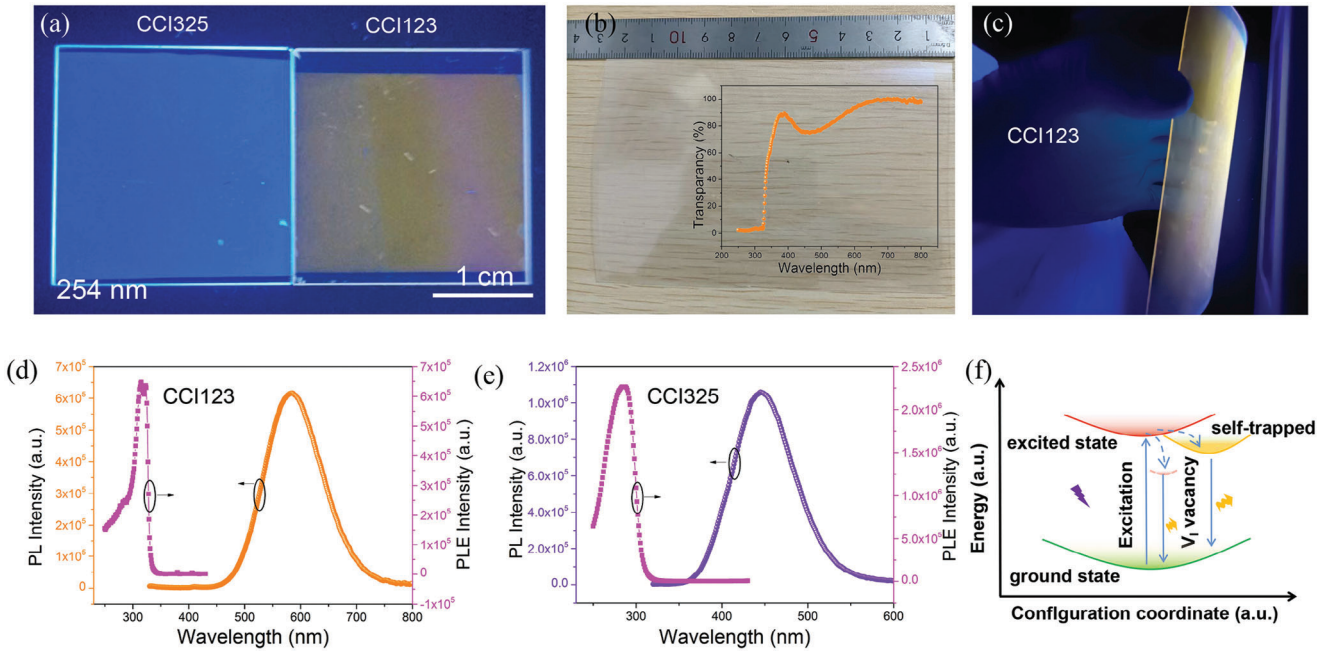

Figure 2. a) Optical image of CCI123 and CCI325 under 254 nm illumination. b) Optical image of CCI123 film on PET substrate and the inset is the corresponding transmission spectrum. c) Flexible CCI123 film under 254 nm illumination. d,e) PL and PLE spectra of CCI123 and CCI325, respectively. f) Illustration of relaxation mechanism of the visible emission of CCI123 and CCI325.

(440), and (190) planes of $CsCu_2I_3$ (PDF # 45–0076).[16] The SEM morphology of CNO nanosheets shown in Figure 1c demonstrated the average size of the nanosheet is 1–3 μm, the regular arrangement of diffraction spots showed its single crystalline properties (inset of Figure 1c), and the HRTEM image with a d spacing of 0.38 nm (Figure S2, Supporting Information) can be ascribed to the (100) face of CNO nanosheets. The AFM images (Figure 1d) further reveal that the thickness of the CNO nanosheet is ≈2.5 nm. To show the uniformity of the CNO and CCI123 films, SEM and AFM images are performed as shown in Figure 1e,f. The CNO nanosheets formed a homogeneous CNO film with a smooth surface (the average roughness R_q is 4.5 nm) on PET substrate (Figure 1e) and the average roughness R_q of CCI123 is 5.1 nm (Figure 1f). The EDS mapping (Figure S3, Supporting Information) of the heterojunction further confirmed the evenly distribution of CNO and CCI123 film. The average thickness of CNO and CCI123 films are ≈502 and 203 nm, respectively (Figure 1g). The UV–vis spectra of CNO, CCI123, and CCI325 in the range of 250–800 nm are illustrated in Figure 1h. The CNO film exhibits an absorption peak at ≈270 nm and the CCI films exhibit an absorption peak at ≈320 nm, indicating that these films may respond to UVC light for photodetectors. And the corresponding calculated energy bandgap of CNO, CCI123, and CCI325 are 4.02, 3.70, and 3.76 eV, respectively (inset of Figure 1h). According to the previous report of the energy band alignment of CCI123 and CNO nanosheets,[11,20] a type-II heterojunction is formed between them as shown in Figure 1i.

It is obvious that under the excitation of 254 nm UVC light, the blue and yellow light can be seen in CCI325 and CCI123 films (**Figure 2**a), respectively. The films can be deposited on a flexible PET substrate, as shown in Figures 2b,c and S4 (Supporting Information). As shown in Figure 2b,c, a large area (≈13×8 cm) CCI on PET substrate with high transparency (> 80%; inset of Figure 2b) was successfully fabricated, demonstrating their potential in flexible perovskite scintillators for X-ray detection. The optical properties of CCI films were further studied by photoluminescence (PL) emission spectroscopy. The CCI123 and CCI325 films with PL excitation peaks centered at 320 and 280 nm, respectively, demonstrate their potential to respond to UVC light (Figure 2d,e). Furthermore, the corresponding broadband PL peaks centered at 584 (CCI123, Figure 2d) and 445 nm (CCI325, Figure 2e), which is consistent with the color of the CCI123 and CCI325 we observed before. Figure 2f depicts a possible PL mechanism of the CCI films. The UV-excited free electrons will transfer into the lower self-trapped state and I vacancy state (V_I).[16,21] Thus, the trapped electrons combine with holes left in the ground state, which contribute to their broadband emission.

The photodetection performance tests of Au/CCI123/Au, Ag/CNO/Ag, and Ag/CNO/CCI123/Au PDs were performed individually. **Figure 3**a–c displays the current–voltage (I–V) curves of Au/CCI123/Au, Ag/CNO/Ag, and Ag/CNO/CCI123/Au PDs, respectively. All the PDs exhibit UV light response abilities. The approximately symmetrical curve shows the approximate ohmic contact of Au/CCI123/Au and Ag/CNO/Ag, while Ag/CNO/CCI123/Au PD demonstrates obvious rectification characteristics with self-powered UVC light photodetection abilities. We can further confirm that a built-in electric field is formed between CNO and CCI123. Parts d and e of Figure 3 show that the photocurrent and responsivity (R) increase with an increase of the applied bias, and the highest R ($R = \frac{I_l - I_d}{PA}$, where I_l and I_d are the photo and dark current, respectively, P is the light intensities and A is the active area) of 1273 mA W^{-1} is obtained at a 3 V

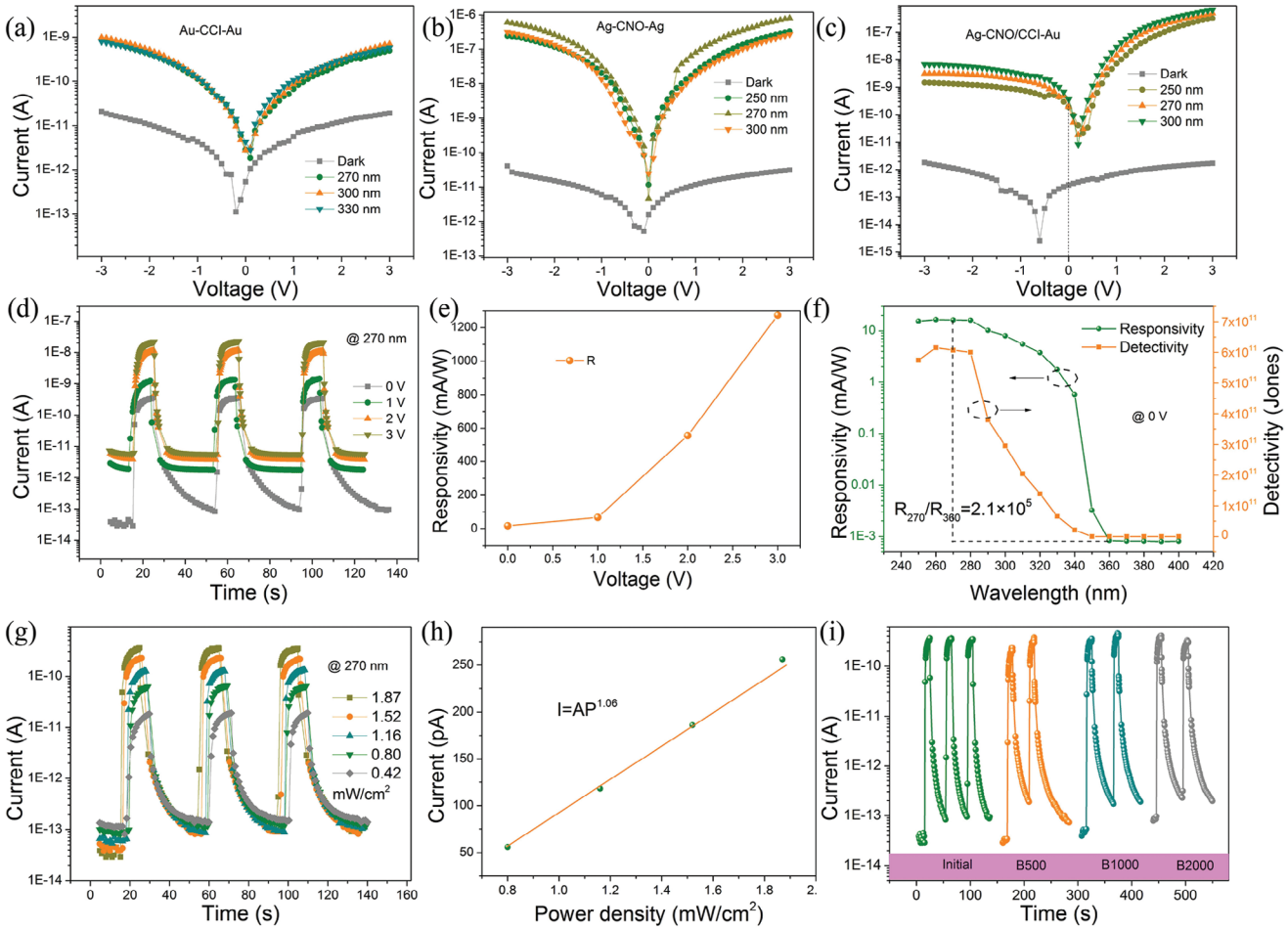

Figure 3. a–c) Current- voltage curves of CCI123, CNO, and CCI123/CNO heterojunctions under dark and UV illumination. d) Current-time (I-t) curves of CCI123/CNO heterojunctions at 270 nm from 0 V to 3V. e) Responsivity of the PD with different voltage. f) Responsivity and detectivity of the PD at 0 V bias. g) I-t curves of the PD under different light intensities at 270 nm. h) Photocurrent dependent on light intensities. i) I-t curves of the PD with various bending times.

bias (270 nm; 1.87 mW cm^{-2}).[21–24] Both the response time and decay time consist of a fast-response as well as a slow-response process. Commonly, the fast-response process is attributed to the rapid change of carriers when the light is on/off (the carriers transmit from the valence band to the conduction band or the reverse process) and the slow-response is own to the trapping/releasing process of carriers caused by the oxygen vacancies in CNO films. The fitted τ_{r1}, $\tau_{r2,}$ τ_{d1}, and τ_{d2} are 0.79, 3.12, 4.24, and 20.6 s, respectively, as shown in Figure S5 (Supporting Information).

The photodetection ability of Ag/CNO/CCI123/Au at 0 V was further tested to evaluate its self-powered performance (which was caused by the type II heterojunction formed between CCI123 and CNO films). Figure S6 (Supporting Information) shows the current-time (I-t) curve of the spectral response of Ag/CNO/CCI123/Au PD under 0 V; the corresponding calculated R (left axis) and detectivity (D*, right axis, $D^* = \frac{R}{(2eI_d/A)^{1/2}}$, e = 1.6×10^{-19} C) values are shown in Figure 3f.[25–27] High self-powered R values of 16.7 mA W^{-1} (at 270 nm) and D* values of 6.1×10^{11} Jones were attained. In the meantime, a self-powered EQE with a value of 7.5% is obtained (@270 nm, 0 V bias), as shown in Figure S7 (Supporting Information). Moreover, an ultrahigh rejection ratio (R_{270}/R_{360}) with a value of 2.1×10^5, demonstrated its excellent UVC detection ability. Figure 3g is the I-t curves of Ag/CNO/CCI123/Au PD performed at different light intensities (270 nm; 0 V). The photocurrent increased with the increasing UVC light intensity, a highest on/off ratio with a value of 3789 was obtained when the light intensity is 1.87 mW cm^{-2}. The corresponding dependence of photocurrent on light intensity ($I = P^{\theta}$) is shown in Figure 3h.[28,29] The fitted θ is 1.06 demonstrate the less recombination ratio of the photogenerated carriers. Due to the flexibility and stability of the 2D CNO nanosheet, the photodetection performance of the Ag/CNO/CCI123/Au PD remains unchanged after 2000 cycles of bending (Figure 3i) and 2 months of restoration in N_2 atmosphere (Figure S8, Supporting Information). Only a little photocurrent (96.7% photocurrent maintenance) decreased when the PD are maintained in air for 7 days(Figure S8, Supporting Information). The performance of our PD is comparable or better than the UVC PDs in the literature as we compared in Table S1 (Supporting information).

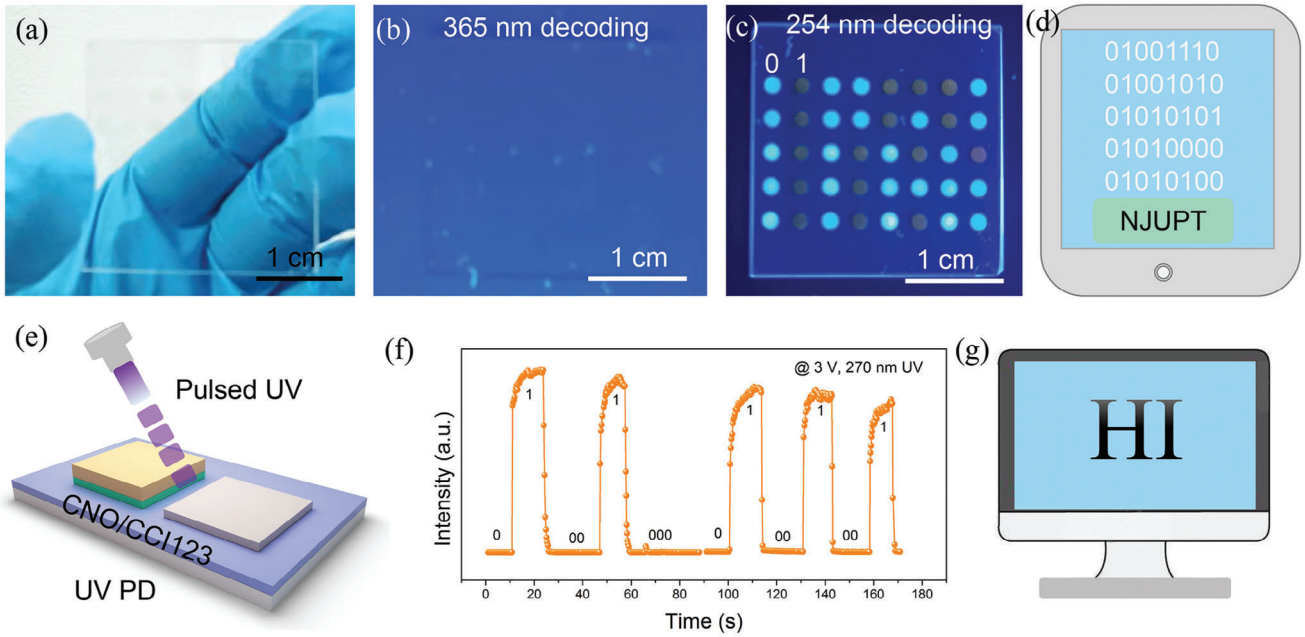

Figure 4. a–c) The confidential information under daylight, 365 nm light, and 254 nm light, respectively, (the blue dots under 254 nm light are generated by CCI325, and the yellow dots are generated by CCI123). And d) is the corresponding decoded information. e) The UVC PD under tuned UVC light and the corresponding electrical signals (in linear coordinates) f). g) The decoded information from the electrical signals.

The majority of UVC light is absorbed by the ozone layer, resulting in rare transmission to the earth's surface. Therefore, the utilization of UVC light to transmit information ensures a highly secure dissemination of data. A piece of quartz glass with information is shown in **Figure** 4a. There is nothing can be observed when using 365 nm UVC light to decode the information (Figure 4b). When we further used 254 nm UV light to decipher the information, regular blue and yellow dots appeared (Figure 4c). A set of data can be obtained by defining the blue dot as "0" and the yellow dot as "1". The "NJUPT" information can be got through binary password decoding (Figure 4d). In addition, the stored information can still be decoded by UVC light even after being stored in the drying oven for 8 months (Figure S9, Supporting Information). Besides, the information can be further transmitted by recording electrical signals. When a series of regulated UVC light irradiates the PD (Figure 4e), the corresponding electrical signal changes can be obtained. The dark current signal is recorded as "0", the photocurrent signal is recorded as "1" (Figure 4f), and the message "HI" can be obtained (Figure 4g), so as to realize the safety transmission of information.[30,31]

The vivid-display image behavior of CCI films and the Ag/CNO/CCI123/Au PD were carried out to validate their imaging capabilities. The mask with special morphology (UVC shape) is placed between the UVC light and the CCI films (**Figure** 5a; Figure S10, Supporting Information). When the UVC light shines on the film through the mask, it will produce yellow (CCI123; Figure 5b) or blue (CCI325; Figure 5c) light visible to the naked eye with high stability even after 8 months(Figure S11, Supporting Information), which can realize the real-time imaging and early warning of UVC light. Furthermore, a UVC imaging system based on the Ag/CNO/CCI123/Au PD was further built as shown in Figure 5d. The template moves in the direction of x and y, and the PD combined with the Keithley 4200 is used to record the changes of light and dark current.[32–35] The results (Table S2, Supporting information) and the corresponding obtained 2D image is shown in Figure 5e, achieving the purpose of UV imaging. The dual-detectable of UVC light based on CNO nanosheets and CCI films realized two ways of UVC light communication and imaging, respectively, which may have great application potential in the UVC light detection prospects.

3. Conclusion

In conclusion, a flexible dual-detectable ultraviolet band C photodetector (UVC PD) based on $Ca_2Nb_3O_{10}$ nanosheets and $CsCu_2I_3$ film was successfully fabricated on a PET substrate in our work. The PD demonstrated a high self-powered UVC light (270 nm; 1.87 mW cm^{-2}) detection abilities with a responsivity (16.7 mA W^{-1}), detectivity (6.1×10^{11} Jones), on/off ratio (3789), ultra-high UVC/UVA (R_{270}/R_{360}) rejection ratio (2.1×10^5), and ultra-stable flexible photodetection abilities. Furthermore, it can turn the UVC light into visible light immediately, realizing the real-time monitoring of UVC light. The dual-detectable PD can be well applied in safety communication and imaging. The results obtained in our study pave a new way in the fabrication of new types of UVC PDs.

4. Experimental Section

Fabrication of $Ca_2Nb_3O_{10}$ and CCI Films: The CNO nanosheets were fabricated by a calcination-exfoliation method according to the previous report. The K_2CO_3 (99.99%), $CaCO_3$ (99.99%), and Nb_2O_5 (99.99%) with

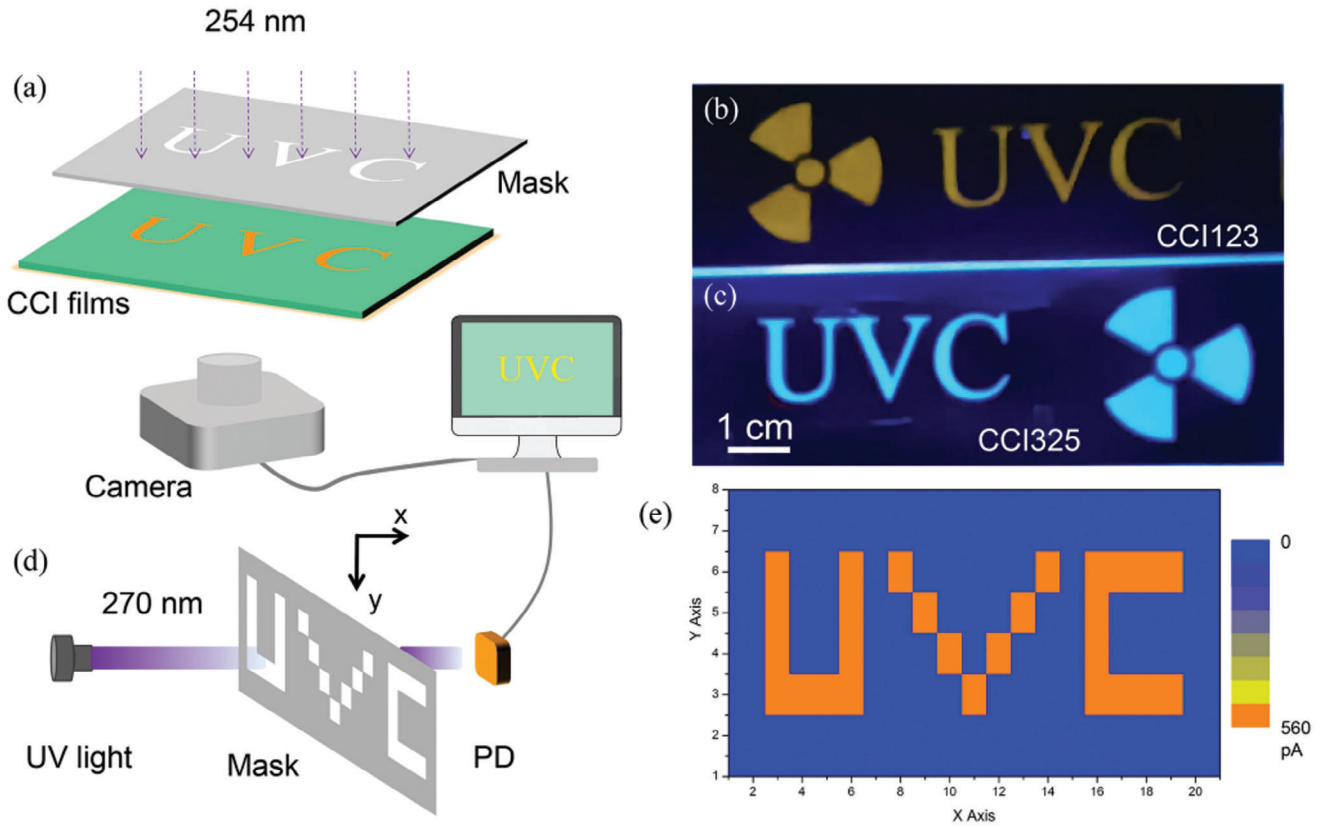

Figure 5. a) UVC imaging demonstration using the CCI123 and CCI325 film and the corresponding imaging results b,c). d) A single pixel (CNO/CCI123) UVC imaging system and the results e).

a molar ratio of K:Ca:Nb = 1.05:2:3 was mixed and ground for 30 min, and calcinated at 950 °C for 1 h in the atmosphere. The product was fully ground for 30 min again and then calcinated at 1150 °C for 10 h in the atmosphere. 0.3 g synthesized $KCa_2Nb_3O_{10}$ and 15 mL 5 m HNO_3 were mixed and stirred for 3 days and the acid was changed every 24 h to get the $HCa_2Nb_3O_{10}$. The $HCa_2Nb_3O_{10}$ was washed many times with deionized water to remove HNO_3 before dispersion in aqueous solution with an equimolar amount of tetrabutylammonium hydroxide solution (TBAOH, 25% aqueous solution). The CNO nanosheets were got by shaking the solution for 7 days. The obtained CNO nanosheets were washed with distilled water for three times and exposed to UV light to remove the TBA^+ before use. For the fabrication of CCI films, the CsI (99.99%) and CuI (99.9%) with a molar ratio of 1:2 (named as CCI123) and 3:2 (named as CCI325) were ground for 1 h. Then 0.5 g mixed powders were evaporated under vacuum condition (10^{-5} Pa) to form a 200 nm film at a constant rate of 0.2 nm s^{-1}.

Materials Characterization: The crystal structure, and morphology of the materials and films were characterized by X-ray diffraction (XRD; $\lambda = 0.15418$ nm), field-emission scanning electron microscopy equipped with energy-dispersive X-ray spectroscopy (EDS) (TESCAN MIRA LMS), transmission electron microscopy (ThermoFisher Talos F200X), and AFM (Bruker Dimension Icon). The thickness of the film was tested using a Step Profiler. Absorption and photoluminescence spectra were collected by an UV–vis spectrophotometer (UV2450, Shimadzu) and an FLS920 fluorescence spectrometer.

Device Fabrication and Photoelectric Measurements: For flexible devices, PET substrates were treated with 5 min plasma before coating CNO films. The CNO nanosheet dispersion was drop-coated on the substrate and then dried at 60 °C in air. The CCI123 film was evaporated on the CNO layer through a shadow mask, and then Au and Ag electrodes were deposited on the CCI123 and CNO film, respectively. The photodetection performance tests of the PD were conducted on a Keithley 4200 equipped with an Xe lamp and a monochromator.

Supporting Information

Supporting Information is available from the Wiley Online Library or from the author.

Acknowledgements

This work is supported by the National Natural Science Foundation of China (No. 62374035, 52425308, 52402191, and 92263106), the Special Basic Research Fund of Jiangsu Province (No. BK20240633), the General Projects of Basic Scientific Research in Colleges and Universities of Jiangsu Province (No. 24KJD430007), the Natural Science Research Start-up Foundation of Recruiting Talents and the Project of State Key Laboratory of Organic Electronics and Information Displays of Nanjing University of Posts and Telecommunication (No. NY223177, GZR2024010026). The authors thank Dr. Xinglong Zhang for his kind help in this manuscript.

Conflict of Interest

The authors declare no conflict of interest

Data Availability Statement

The data that support the findings of this study are available in the supplementary material of this article.

Keywords

dual-detectable, lead-free perovskites, real-time imaging, safety communication, UVC photodetector

Received: November 14, 2024
Revised: December 20, 2024
Published online:

[1] a) S. Li, X. Liu, H. Yang, H. Zhu, X. S. Fang, *Nat. Electron.* **2024**, *7*, 216. b) D. Wang, X. Liu, Y. Kang, X. Wang, Y. Wu, S. Fang, H. Yu, M. H. Memon, H. Zhang, W. Hu, Z. Mi, L. Fu, H. Sun, S. Long, *Nat. Electron.* **2021**, *4*, 645.
[2] a) X. Zhou, Z. Lu, L. Zhang, Q. Ke, *Nano Energy* **2023**, *117*, 108908; b) Y. Hu, Z. Q. Li, X. S. Fang, *J. Inorg. Mater.* **2023**, *38*, 1055.
[3] a) Z. Li, T. Yan, X. S. Fang, *Nat. Rev. Mater.* **2023**, *8*, 587. b) F. Cao, Y. Liu, M. Liu, Z. Han, X. Xu, Q. Fan, B. Sun, *Research* **2024**, *7*, 0385.
[4] a) S. Cai, C. Zuo, J. Zhang, H. Liu, X. S. Fang, *Adv. Funct. Mater.* **2021**, *31*, 2100026. b) D. Wang, W. Wu, S. Fang, Y. Kang, X. Wang, W. Hu, H. Yu, H. Zhang, X. Liu, Y. Luo, J.-H. He, L. Fu, S. Long, S. Liu, H. Sun, *Light Sci. Appl.* **2022**, *11*, 227.
[5] a) J. Chen, X. Liu, Q. Zhu, X. S. Fang, W. Xu, *Adv. Funct. Mater.* **2024**, *34*, 2402684. b) H. Zhang, F. Liang, K. Song, C. Xing, D. Wang, H. Yu, C. Huang, Y. Sun, L. Yang, X. Zhao, H. Sun, S. Long, *Appl. Phys. Lett.* **2021**, *118*, 242105.
[6] S. Huang, J. Lin, X. Lin, Z. Wang, Y. Xie, X. Chen, X. Kong, W. Zheng, Q. Hu, *ACS Appl. Mater. Interfaces* **2023**, *15*, 37649.
[7] C. Lin, Z. Zhang, Y. Lu, X. Yang, Y. Zhang, X. Li, J. Zang, X. Pang, L. Dong, C. Shan, *Carbon* **2022**, *200*, 510.
[8] B. Uppalapati, D. Gajula, F. Bayram, A. Kota, A. Gunn, D. Khan, V. P. Chodavarapu, G. Koley, *ACS Photonics* **2022**, *9*, 1908.
[9] Y. Zhou, Z. Zhang, X. Yang, T. Liu, G. He, C. Lin, W. Huang, H. Liu, Y. Wang, Y. Wang, Z. Xiang, C. Shan, *ACS Nano* **2024**, *18*, 7610.
[10] S. Cai, X. Xu, W. Yang, J. Chen, X. S. Fang, *Adv. Mater.* **2019**, *31*, 1808138.
[11] Y. Zhang, S. Li, Z. Li, H. Liu, X. Liu, J. Chen, X. S. Fang, *Nano Lett.* **2020**, *21*, 382.
[12] S. Li, Y. Zhang, W. Yang, H. Liu, X. S. Fang, *Adv. Mater.* **2020**, *32*, 1905443.
[13] F. Cao, E. Hong, Z. Hu, Y. Liu, B. Sun, J. He, X. S. Fang, *Nano Energy* **2024**, *120*, 109135.
[14] a) Y. Zhang, F. Cao, S. Y. Li, X. Y. Liu, L. X. Kang, L. M. Wu, X. S. Fang, *J. Mater. Sci. Technol.* **2022**, *129*, 108. b) F. Cao, L. Jin, Y. Wu, X. Ji, *J. Alloys Compd.* **2021**, *859*, 158383.
[15] J. Wang, Y. Zhang, J. Chen, Y. Wei, D. Yu, L. Liang, Y. Liu, Y. Wu, W. Shen, X. Li, H. Zeng, *ACS Appl. Mater. Interfaces* **2021**, *13*, 36147.
[16] S. Han, J. Quan, D. Wang, H. Li, X. Liu, J. Xu, Y. Zhang, Z. Li, L. Wu, X. S. Fang, *Adv. Sci.* **2023**, *10*, 2206417.
[17] J. Lv, X. Lu, X. Li, M. Xu, J. Zhong, X. Zheng, Y. Shi, X. Zhang, Q. Zhang, *Small* **2022**, *18*, 2201715.
[18] Q. Lu, Y. Zhang, G. Yang, M. Xiong, W. Wu, Z. Xu, H. Lu, Y. Liang, Z. He, Y. Yu, X. Mo, X. Han, C. Pan, *Small* **2023**, *19*, 2300364.
[19] X. Liu, S. Li, Z. Li, F. Cao, L. Su, D. V. Shtansky, X. S. Fang, *ACS Appl. Mater. Interfaces* **2022**, *14*, 48936.
[20] X. Deng, Z. Li, F. Cao, E. Hong, X. S. Fang, *Adv. Funct. Mater.* **2023**, *33*, 2213334.
[21] K. Zhang, S. Wang, L. Yi, *J. Lumin.* **2023**, *254*, 119516.
[22] a) F. Cao, Z. Li, X. Liu, Z. Shi, X. S. Fang, *Adv. Funct. Mater.* **2022**, *32*, 2206151; b) L. Min, H. Sun, L. Guo, Y. Zhou, M. Wang, F. Cao, L. Li, *Adv. Mater.* **2024**, *36*, 2400279.
[23] a) Y. Chen, X. Yang, P. Sun, W. Dou, X. Chen, C. Zhang, C. Shan, *Mater. Horiz.* **2021**, *8*, 3368; b) L. Min, H. Sun, L. Guo, M. Wang, F. Cao, J. Zhong, L. Li, *Nat. Commun.* **2024**, *15*, 2066.
[24] A. R. Jayakrishnan, J. P. B. Silva, K. Gwozdz, M. J. M. Gomes, R. L. Z. Hoye, J. L. MacManus-Driscoll, *Nano Energy* **2023**, *118*, 108969.
[25] F. Cao, Z. Hu, T. Yan, E. Hong, X. Deng, L. Wu, X. S. Fang, *Adv. Mater.* **2023**, *35*, 2304550.
[26] M. Ding, K. Liang, S. Yu, X. Zhao, H. Ren, B. Zhu, X. Hou, Z. Wang, P. Tan, H. Huang, Z. Zhang, X. Ma, G. Xu, S. Long, *Adv. Opt. Mater.* **2022**, *10*, 2200512.
[27] H. Sheoran, S. Fang, F. Liang, Z. Huang, S. Kaushik, N. Manikanthababu, X. Zhao, H. Sun, R. Singh, S. Long, *ACS Appl. Mater. Interfaces* **2022**, *14*, 52096.
[28] F. Cao, X. Deng, X. Liu, L. Su, E. Hong, L. Wu, X. S. Fang, *ACS Appl. Mater. Interfaces* **2023**, *15*, 28158.
[29] F. Cao, T. Yan, Z. Li, L. Wu, X. S. Fang, *Adv. Opt. Mater.* **2022**, *10*, 2200786.
[30] S. Fang, L. Li, W. Wang, W. Chen, D. Wang, Y. Kang, X. Liu, H. Jia, Y. Luo, H. Yu, M. H. Memon, W. Hu, B. S. Ooi, J. H. He, H. Sun, *Adv. Mater.* **2023**, *35*, 2300911.
[31] W. Chen, D. Wang, W. Wang, Y. Kang, X. Liu, S. Fang, L. Li, Y. Luo, K. Liang, Y. Liu, D. Luo, M. H. Memon, H. Yu, W. Gu, Z. Liu, W. Hu, H. Sun, *Adv. Mater.* **2024**, *36*, 2307779.
[32] L. Li, H. Y. Chen, Z. M. Fang, X. Y. Meng, C. T. Zuo, M. L. Lv, Y. Z. Tian, Y. Fang, Z. Xiao, C. X. Shan, Z. G. Xiao, Z. W. Jin, G. Z. Shen, L. Shen, L. M. Ding, *Adv. Mater.* **2020**, *32*, 1907257.
[33] D. Wu, M. Xu, L. Zeng, Z. Shi, Y. Tian, X. J. Li, C. X. Shan, J. Jie, *ACS Nano* **2022**, *16*, 5545.
[34] J. K. Qin, H. Xiao, C. Y. Zhu, L. Zhen, C. Y. Xu, *Adv. Opt. Mater.* **2022**, *10*, 2201627.
[35] W. Wang, W. Wang, Y. Meng, Q. Quan, Z. Lai, D. Li, P. Xie, S. Yip, X. Kang, X. Bu, D. Chen, C. Liu, J. C. Ho, *ACS Nano* **2022**, *16*, 11036.